Simulation of damage observed on buildings in aggregate after the 2016-2017 Central Italy earthquake accounting for site effects and soil-structure interaction

A. Brunelli
University of Genova

G.A. Alleanza
University of Naples Federico II

S. Cattari
University of Genova

F. de Silva & A. d'Onofrio
University of Naples Federico II

ABSTRACT: The paper investigates the influence of site effects and soil-structure interaction on the response of buildings in aggregate in the historical centre of Visso, located in an alluvial valley in the Central Italy. The town was severely stricken by the Central Italy 2016/2017 seismic sequence and the subsequent inspections allowed the reconnaissance of damage suffered by the case study at hand. A monitoring system installed just out of the historical centre recorded the ground motion at Visso during the seismic sequence. Based on these records, the bedrock motion was then calculated through their deconvolution along the well characterized soil profile below the record station. The resulting signals were applied as input motions in linear equivalent site response analyses (i) of the 1D soil stratigraphy below the buildings in aggregate and (ii) of the whole 2D valley. In both cases, the subsoil model was inferred from the data gathered during the seismic microzonation study of the Visso village. The amplification of ground motion resulting from the 1D site response analysis is higher than that predicted by the 2D analysis along the same vertical. The whole aggregate was modelled in the Tremuri software through the equivalent frame approach and specific modelling strategies were adopted to account for the interaction among adjacent structural units. The model base was either completely restrained, to simulate the fixed-base conditions as typically assumed in the structural analysis, or endowed with springs, to simulate the effect of the soil compliance to the structural motion. Non-linear dynamic analyses were then performed on the fixed and complaint base models under the free-field motion obtained from the 1D and 2D site response analyses. The resulting damage patterns were compared to that detected on site. The comparison is satisfying only when the motion obtained from 2D site response is adopted as input motion and slightly improved when the compliant base conditions are considered.

1 INTRODUCTION

Ancient towns were often built to be isolated from the surroundings, mainly due to defensive strategies. Hence, they usually rise on flat-topped hills delimited by steep slopes or in valleys enclosed by mountains. Such complex geomorphological conditions influence the ground motion at surface (Pagliaroli et al. (2020)). This especially occurs in the case of valley, where also stratigraphic amplification effects are expected to be produced by soft covers. Moreover, the seismic response of structures founded on such covers is potentially also modified by the soil-structure interaction (Richart et al. (1970)). Such phenomena were recently investigated for unreinforced masonry (URM) buildings by Brunelli et al. (2021) through the in-depth analysis of the response of the school of Visso (MC, Italy). The school constitutes an emblematic example hit by the Central Italy 2016/2017 seismic events and provided very precious and unique information, being permanently monitored by the Italian Department of Civil Protection. Other works based on evidence from recent earthquakes have already highlighted the detrimental effects of site-amplification in the damage of existing URM masonry buildings (for example: Sextos et al. (2018); Sorrentino et al. (2019); Brando et al. (2020)). Soil-foundation-structure (SFS) interaction is often

not considered for URM buildings with shallow foundations, while Brunelli et al. (2022) showed the role of the interaction and the susceptibility of the results to variation of different formulations in the literature. This paper numerically investigates the effect of site amplifications and SFS interaction on the response of a building in aggregate located in the historic center of Visso to the Central Italy 2016-2017 seismic sequence. Actually, studies on URM buildings in aggregate, that also consider the role of SFS interaction, are very few in literature (Caprili et al. (2015)). The aggregate is modelled taking advantage from the validation of the equivalent frame modelling strategy carried out by Brunelli et al (2021) on the Visso's school and refining the strategy with *ad hoc* solutions to account for the interaction between adjacent structural units, as recently investigated in Angiolilli et al. (2021). Being the case study settled not far from the border of the valley, an attenuation of the seismic motion is expected with respect to the 1D condition, due to the destructive interference among the refracted waves along the edges (Alleanza et al. (2019); Papadimitriou (2019)). Thus, an *ad hoc* study on this issue has been also performed in the paper. The agreement in terms of simulated damage is adopted as target to assess the role of various phenomena. Indeed, the influence of SFS interaction is expected to be beneficial, thanks to the contribution of damping associated to continuous and shallow foundation of such URM structure.

2 DESCRIPTION OF THE CASE STUDY

The investigated building in aggregate is made up of five units placed in rows having varying heights, from three to four floors. Due to the impossibility to make a detailed geometric survey of the buildings, their size was deduced from the photos and maps of Visso (see https://www.regione.marche.it/Regione-Utile/Paesaggio-Territorio-Urbanistica/Cartografia/Repertorio/Cartatecnica2000). The reconstructed geometry of the aggregate is reported in Figure 1.

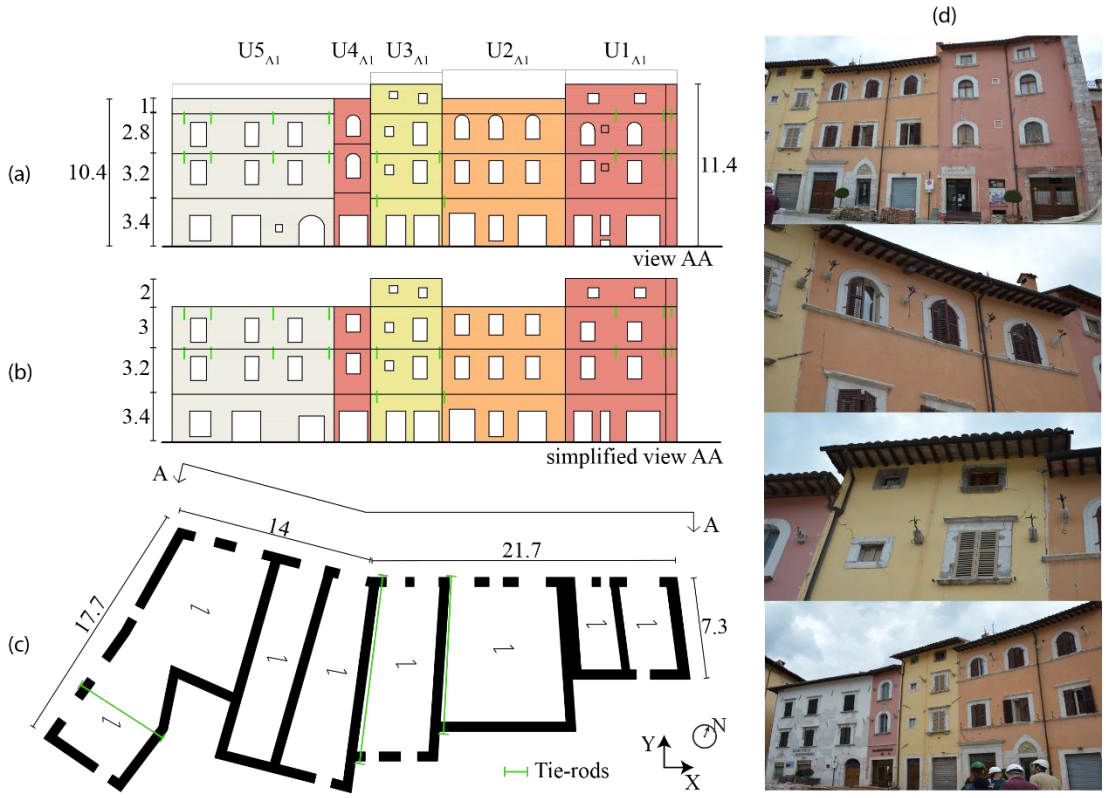

Figure 1. Geometric survey of building in (a) the real, (b) simplified elevation and (c) in plan of the ground floor; (d) photo of the aggregate following the seismic events in Central Italy 2016/17.

The height of the floors was inferred from the position of the openings and tie-rods visible from outside. Some structural features were deduced from other buildings where partial collapses, induced by out-of-plane mechanisms, occurred. Such collapses made these details visible, allowing

to also verify their systematic recurrence (see Figure 2). Firstly, in such way, the transversal sections of URM walls were investigated by deducing the thickness and the masonry type. Indeed, the latter is mostly the same across the historical centre and is also consistent with that of the school of Visso (see Brunelli et al. (2021)). Basing on such evidence, the walls were estimated 70 cm thick at the ground floor and 60 cm at the other levels. The only exceptions are the perimeter wall of unit $U1_{A1}$ (the right wall in Figure 1c) estimated 80 cm thick over the entire height of the building; and the walls of the last level in 55 cm. Moreover, the presence of internal walls was assumed in correspondence of the tie-rods visible in the external façades. The internal walls were supposed 5 cm lower as thickness than the relative perimeter walls. Basing on the position of the tie-rods and the typology of the single units, the units $U1_{A1}$ and $U2_{A1}$ are assumed to be sustained by autonomous load-bearing walls, while the other units to share the side transversal walls (i.e. those oriented in Y direction). In particular, the unit $U4_{A1}$ seems to be a filling unit built upon the two pre-existing orthogonal walls.
The main orientation of diaphragms is expected to develop perpendicularly to the Y-direction; all partition masonry walls were considered in the model as equivalent loads on the floors. From the photos of the other buildings in the historic center (see Figure 2), diaphragms are mostly characterized by brick and wooden decks. In some case, a very thin concrete slab (not reinforced) is also present. The same floor type was assumed in all units of the aggregate under examination since there is no evidence of any specific interventions and the units are considered substantially contemporary.

Figure 2. Example of walls and floors visible in other buildings of the historic center of Visso.

3 SITE EFFECTS IN THE VALLEY OF VISSO

3.1 *Subsoil geotechnical model*

The examined buildings in aggregate are on the border of an alluvial valley, whose 2D geological section is shown in Figure 3a (MZS3 (2018)). The soil stratigraphic sequence under the aggregate was defined thanks to the data of two boreholes and several Horizontal to Vertical Spectral Ratio (HVSR) of microtremors carried out within the third level microzonation studies, MZS3 (2018). The soil profile is constituted by clayey silt (CS), overlaying a sandy gravel layer (SG). In lack of experimental measurements, the shear wave velocity profile (V_S) was obtained through a correlation law between V_S and the number of blow counts of SPT tests performed in the boreholes. To validate the model, several correlations available in literature were checked and compared with the results of a Down Hole test (DH) carried out in a different site within the valley. In particular, the correlations by Imai & Yoshimura (1970) and Lee (1992) were used for CS and the one suggested by Ohta & Goto (1978) was adopted for SG, Figure 3b,c shows respectively the V_s profiles obtained for the two verticals V1 and V2, and used to define the geotechnical model for the seismic response analysis. The V1 profile (Figure 3b) was used to characterise the widest and thickest valley below the school, while the V2 (Figure 3c) profile was adopted for the shallow lateral valley below the aggregate. Each profile was extended to the entire section assuming a horizontal layering. The interface between the two valleys was established in accordance with the results of MZS3 (2018). The shear modulus decay ($G(\gamma)/G_0$) and the variation of damping ratio ($D(\gamma)$) curves (Figure 3d) were assigned based on Brunelli et al. (2021). The relations developed by Ciancimino et al. (2020) for Central Italy soils was used to characterise the non-linear behaviour of CS and SC layers, considering an average value of plasticity index of 17% (measured

on samples retrieved these formations). While for SG layers, the relationships suggested by Liao et al. (2013) were adopted, considering a confining pressure of 52 kPa for the superficial one and 207 kPa for the deeper, to reproduce the dependence of the nonlinear behaviour on the stress state. The bedrock was assumed to be linear visco-elastic with a damping of 0.5% and V_S=1300m/s, in agreement with the results obtained by MZS3 (2018).

The 2D analyses were carried out with the computer code QUAD4M (Hudson et al. (2003)), a finite element program that performs equivalent linear analysis in the time domain. The domain was laterally extended to minimize the effect of artificial reflections of the seismic waves due to lateral boundaries. The mesh consists of triangular elements, whose maximum size was defined according to Kuhlemeyer & Lysmer (1973) criterion. 1D seismic response analyses were also carried out along the vertical profiles V1 and V2 (Figure 3b,c) with the computer code STRATA (Kottke & Rathje (2008)) which performs equivalent linear analysis in the frequency domain.

The reliability of the obtained geotechnical model was checked by comparing the experimental fundamental frequency measured by the HVSR, at several sites along the cross-section of the valley, with that computed at the same site by 1D and 2D linear analyses. Figure 3a shows the comparison between the measured resonance frequencies (in black) and those obtained in the 1D (dark grey) and 2D (light grey) case. The agreement among the frequency values validates the numerical model.

Two-time histories of the Central Italy seismic sequence 2016-17, recorded near the school foundations (Figure 3a) were then used as reference seismic input motion. In particular, the main events of 24/08/2016 and 26/10/2016 were considered. They were deconvoluted at the bedrock through a 1D analysis and then applied to the 2D model of the valley, as well as to the 1D soil column V2 to obtain the ground motion at the base of the aggregate.

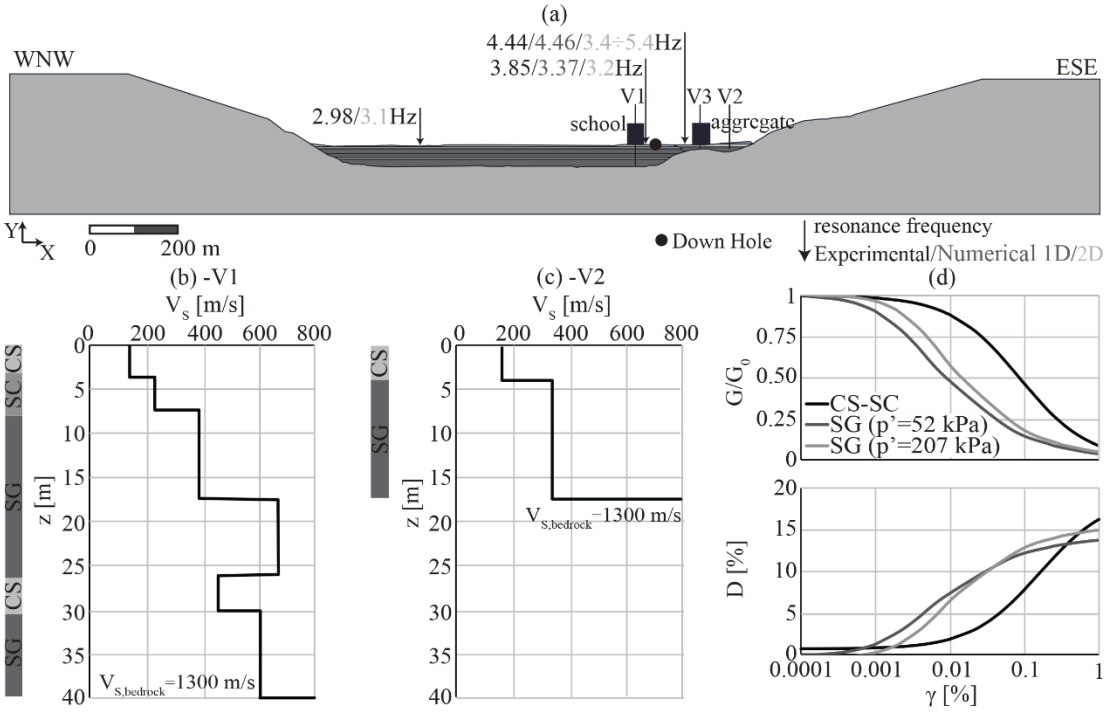

Figure 3. (a) 2D section adopted in the numerical analyses; (b) V_S profiles measured through the down hole test; (c) V_S profiles for the historical center of Visso and (d) G/G_0-γ and D-γ curves adopted in the analyses. Black and grey numbers along the cross-section in the upper portion represent experimental and numerical estimation of first natural frequency respectively (in 1D and 2D case).

3.2 *Results of site response analyses*

The results of the analyses were synthesized in terms of horizontal profiles of the amplification factors of spectral acceleration (AF) defined through equation 1:

$$AF_{T_a-T_b} = \frac{\int_{T_a}^{T_b} S_{a,s}(T)\,dT}{\int_{T_a}^{T_b} S_{a,r}(T)\,dT} \quad (1)$$

where $S_{a,s}(T)$, $S_{a,r}(T)$ are the spectral accelerations at the surface and at bedrock, and T_a, T_b were set equal to 0.1 and 0.5 s. The period range was defined in a way that is almost centred on the natural period of the aggregate. Furthermore, an amplification factor of peak ground acceleration, AF_{PGA}, was also calculated.

Figure 4 shows the profiles of $AF_{0.1\text{-}0.5s}$ (solid lines and full dots) and AF_{PGA} (dashed lines and empty dots), computed adopting the two input motions, obtained from both 2D (lines) and 1D (symbols) analyses. The trends of $AF_{0.1\text{-}0.5s}$ and AF_{PGA} between X= 600 m and 1400 m are comparable for the two events and characterized by two amplification peaks located close to the border of the deepest valley. This behaviour is typical of very shallow valleys characterised by a shape ratio, $H/B \leq 0.1$ (Alleanza (2022)). Furthermore, the amplification factors obtained from 1D analysis along V1 profile are close to those computed by 2D analysis, justifying the good agreement between the damage observed at the school and that simulated by Brunelli et al. (2021) adopting the ground motion at surface, obtained from 1D analysis. On the other hand, the thin valley, between X=1400 m and 1600 m, shows a strong amplification of motion at the centre of the basin, leading to amplification higher than that computed by 1D analysis along the vertical V2. Indeed, a destructive wave field among the direct, refracted and surface waves close to the edges of the valley (e. g. V3 in Figure 4) attenuates the ground motion with respect to the centre (Alleanza et al. (2019); Alleanza (2022)). Consequently the spectral amplifications are lower than those predicted by 1D analyses along V2. Finally, nevertheless the differences in the soil profiles, 1D analyses along V1 and V2 lead to close values of the amplification factors, because their seismic response is mainly ruled by the shallowest (up to a depth of 18 m) and softest layers, characterised by similar dynamic properties.

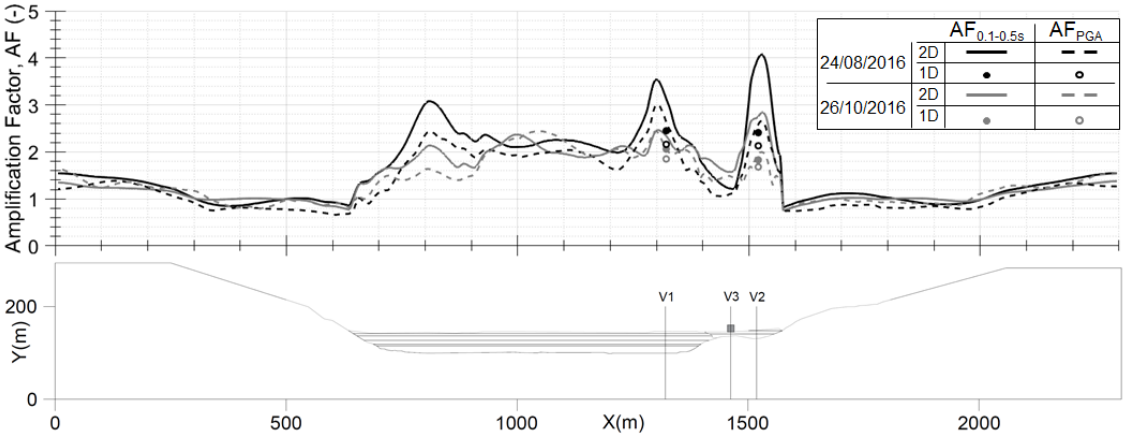

Figure 4. 2D amplification factors of the peak ground acceleration and of the spectral acceleration compared to those computed through 1D seismic response analyses along the verticals V1 and V2.

Figure 5 shows the comparisons among the accelerograms obtained on the surface from 1D (black line) and 2D (grey line) analyses for the events of 24/08/16 (continuous line) and 26/10/16 (dashed line). In details, Figure 5a compares the results at V1; in while Figure 5b compares the results obtained from the 1D analyses at V2 and from the 2D analyses at V3 (Figure 5b), where the aggregate is settled. The latter comparison is reported, because in the eventual lack of the 2D simulation, the ground motion resulting from 1D analyses along the vertical in the center of the valley is considered to be representative of the motion of the whole valley. In agreement with the above observations, the results obtained along the V1 profile by 1D and 2D analyses are very close, both in terms of amplitude and frequency content. On the other hand, accelerations and spectra computed along the V2 profile by 1D analyses show on average higher amplitudes respect to those obtained by 2D analyses.

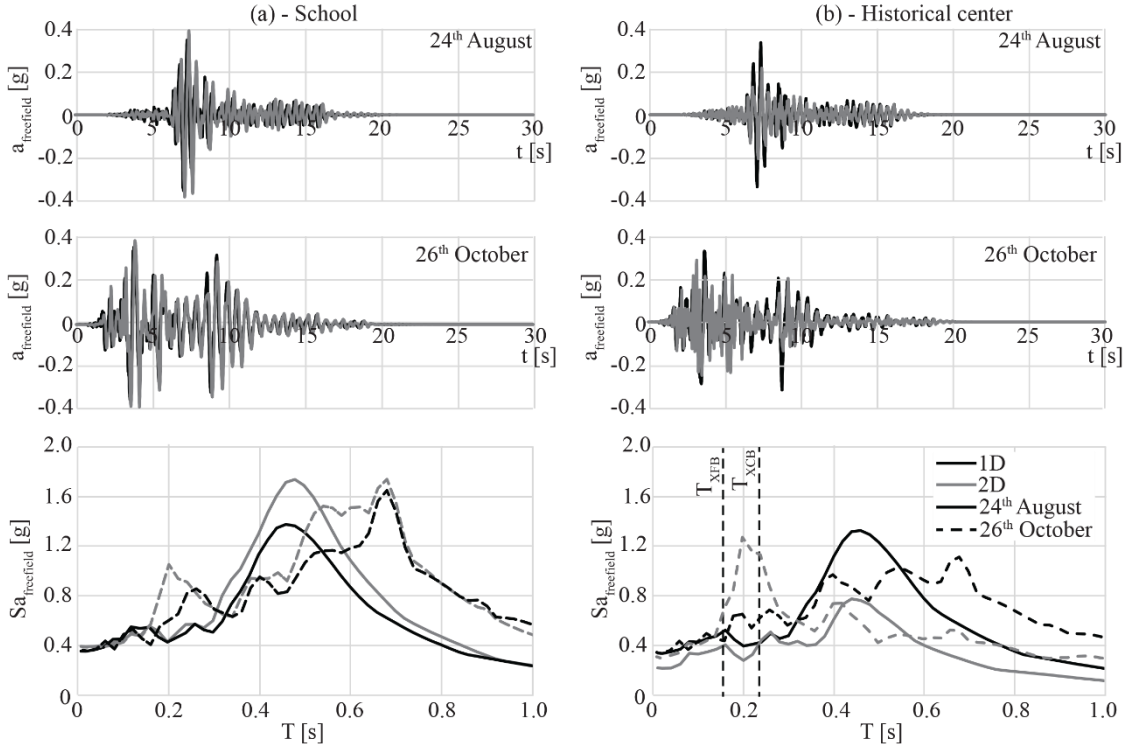

Figure 5. Comparison among the time histories and response spectra of the free field accelerations resulting in (a) school and (b) historical center from the 1D (in correspondence with V1) and 2D (in correspondence with V3) site response analyses under the events occurred on the 24th August and 26th October 2016.

4 EQUIVALENT FRAME MODEL OF BUILDINGS IN AGGREGATE

Among the modelling strategies available for URM structures (see D'Altri et al. (2020)), the 3D model here adopted is based on the equivalent frame approach. Accordingly, the nonlinear behaviour is assumed to be concentrated in masonry panels (the piers and spandrels, in orange and green respectively in Figure 6a) connected by rigid nodes (in cyan in Figure 6a). Piers constitute the main vertical structural elements able to equilibrate both vertical and horizontal actions, while spandrels play the main role of connecting the piers (like the beams in a corresponding reinforced concrete frame). For each URM wall, the geometry of piers and spandrels has been identified *a priori* according to the rules proposed in Lagomarsino et al. (2013), whose reliability has been recently validated in Cattari et al. (2021) and Ottonelli et al. (2021); indeed, the regular layout of openings justifies in this case to neglect such an epistemic uncertainty. The numerical model was realized with the Tremuri software package, developed by Lagomarsino et al. (2013). The model accounts only for the in-plane response of walls, but this simplification is justified in the case of the investigated aggregate that did not exhibit the activation of any local mechanism, differently from other in the historical center.

As far the geometry of the structural units concerns, few simplifications have been made with respect to the original configuration. In particular, the alignment of the floors between the units of the aggregate and the windows have been rectified, by neglecting some small misalignments in height (as shown in Figure 1a). The final view of the assumed geometry is illustrated in Figure 1b.

The adopted values of the Young's modulus (E) and shear modulus (G) are reported in Table 1, together with the strength mechanical parameters. These values have been derived starting from those used in the Visso school, whose reliability has been validated in Brunelli et al. (2021) through a very accurate numerical simulation of the actual response of this monitored asset. The strength values are slightly higher than that used for the school (of a 10%), but still completely consistent with the reference values proposed by Italian Building Code Commentary called MIT

(2019) for the analogous masonry type. Both the elastic modulus and the compressive strength of the spandrels have been reduced by a multiplying factor equal to 0.7 with respect the piers; that is to account for the anisotropic behaviour of masonry and the fact the main mortar joints activated in spandrels are the vertical ones.

Table 1. Mechanical parameters adopted for piers, spandrels and diaphragms of floor.

	E (MPa)	G (MPa)	τ_0 (MPa)	f_m (MPa)	G_D (MPa)	E_D (MPa)
piers	2968	991	0.1268	6.42		
spandrels	2078	693	0.6253	4.94		
diaphragms of floor					9170	23333

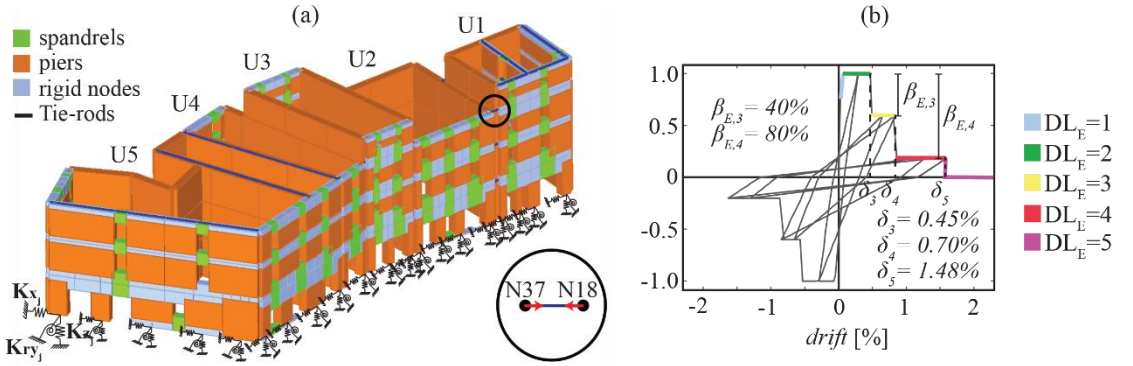

Figure 6. (a) Equivalent frame model; (b) backbone and hysteretic response of the masonry piers under shear.

Masonry panels are modelled according to the nonlinear beam piecewise-linear model proposed by Cattari & Lagomarsino (2013). This constitutive law allows for describing the nonlinear response until very severe damage levels at element scale (i.e. DL_E,i with i from 1 to 5), through progressive strength degradation (β_E,i), corresponding to assigned drift values (δ_i). The latter are differentiated as a function of most recurring failure modes that characterize URM panels (i.e. flexural, diagonal cracking shear or bed-joint sliding) and of their type (if piers or spandrels). They may be defined on basis of experimental dataset available in literature (e.g. Vanin et al. (2017); Rezaie et al. (2020)). In this case, the drift thresholds already validated in Brunelli et al. (2021) have been adopted. By way of example, Figure 6b illustrates the response of a pier dominated by a shear failure mode.

The maximum shear strength of the panels has been computed according to the strength criteria already corroborated in the literature to interpret the aforementioned failure modes (see Calderini et al. (2009)). In particular, the flexural behaviour of piers was interpreted according to the criterion proposed in NTC (2018), whereas the shear behaviour according to the diagonal cracking failure mode proposed by Turnšek & Sheppard (1980) and recommended also in MIT (2019) for existing irregular masonry.

As proposed by Angiolilli et al. (2021), the mutual interaction between the various structural units is considered through the insertion of elastic truss elements (see the circular zoom of Figure 6) and fictitious floors. These elements allow the opening between buildings only along their longitudinal direction (i.e. X direction). The truss element, able to react only in compression, are characterized by a transversal area of 0.00164 m^2 and elastic modulus E of 210000 MPa. The equivalent diaphragms instead are characterized by the following feature: thickness of 0.5 m, E=39420 MPa, G=131125 MPa.

As mentioned in the introduction, two models have been considered. A fixed based (FB) model and compliant base (CB) model to account for the SFS interaction. In the latter case, a series of springs were considered under each pier, as shown in Figure 6a. The details on the calibration of these springs and equivalent Rayleigh damping are given in the next paragraph. Figure 7 shows the fundamental periods of two models together with the in-plan view of the mode shapes, that refer to the FB model. The first period mainly activates the longitudinal response, while the second and third modes the transversal one. More specifically, the second mode substantially involves the units $U1_{A1}$ and $U2_{A1}$, while the third mode the other ones. In the case of the CB model,

the aggregate is idealized through the replacement oscillator approach proposed by Maravas et al. (2014), as better explained in section 4.1. Thus, in this case, two main modes are computed associated to the following periods: 0.221 s for the longitudinal direction; 0.2 for the transversal one.

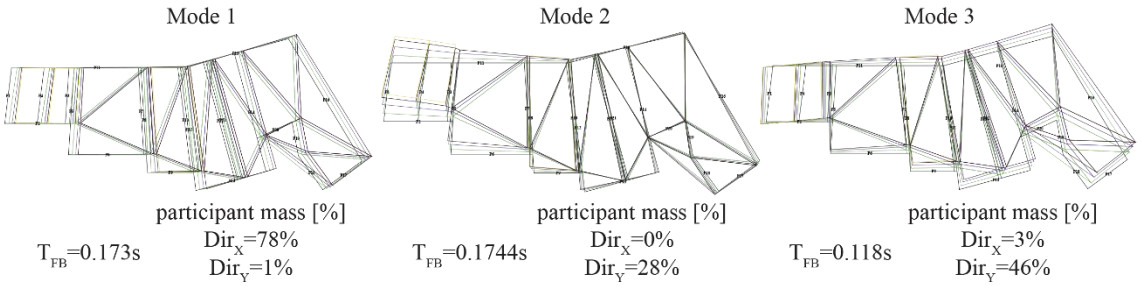

Figure 7. Modal shapes of the first three modes identified of the FB model, with period and participant mass.

4.1 *Modelling of the foundation stiffness and damping*

In the CB model, each foundation pier was equipped with springs, whose stiffness was calibrated through the real part of the soil-foundation impedances by Gazetas (1991). The foundation width was set constant and equal to 1 m, as results from the thickness of the load-bearing wall plus an enlargement of 0.15 m at each side. The length varies because it was defined by adding the half-length of the spandrel panel to the size of the load-bearing wall. The value of the embedment was set to 1 m, in according to the building typology and to the soil type.

The soil was modelled as an equivalent linear half-space. The half-space shear modulus was set equal to mobilized one, under each input motion, up to a depth equal to the foundation width below the foundation, and corresponding to the soil volume expected to be affect by the horizontal and rocking foundation motion (see Gazetas (1983)). As well known, the impedance functions are frequency dependent, hence they were calibrated iteratively until the supposed frequency resulted equal to the inverse of the period of the compliant-base aggregate. The latter was estimated through the replacement oscillator approach proposed by Maravas et al. (2014) for a Single Degree of Freedom (SDoF). To this aim, the building was approximated through a SDoF system with a viscous damping ratio equal to 3%, and a lateral stiffness derived from the fundamental periods along the X and Y directions of the FB configuration. The real and the imaginary parts of the impedance of the monolithic foundation, equivalent to the actual foundation systems, were calculated from the sum of the real or imaginary parts of the impedances of the X-oriented (or Y-oriented) load-bearing walls. Since the cumulative effects of the two mainshock was studied by applying the two input motions in cascade to the numerical model, the mean values of the impedances for each pier were introduced into the base springs of the numerical model.

Figure 8 shows for each foundation the values of the vertical (K_v), horizontal (K_x) and rotational (K_{ry}) impedances calibrated on the initial soil stiffness and on the mobilized one, obtained from the 1D and 2D seismic response analyses. The impedance calibrated on the soil stiffness mobilized into 1D analyses are slightly higher with respect to those associated with the soil stiffness resulting from the 2D analyses. The structural period of CB model is predicted through the formula by Maravas et al. (2014) for the impedances calibrated on the initial soil stiffness.

The same approach by Maravas et al. (2014) was adopted to estimate the damping ratio of the compliant base system. The contribution of the soil hysteretic damping, mobilized in the soil volume affected by the foundation motion, was added to the energy loss coefficients simulating the radiation damping ratio. The mean value of the damping ratio, resulting for the two directions and the two mainshocks, was introduced as a Rayleigh damping ratio into the structural model. Table 2 shows the values for the X and Y direction (equal for the two-subsoil modelling) of the soil damping (D), of the equivalent damping for each direction and event (ξ_{eq}) and of the final value (ξ_{eqTOT}) used in the nonlinear dynamic analyses (NLDA). In general, the hysteretic damping mobilized in the 2D analyses, along the X direction, is slightly higher than that predicted through the 1D analyses, hence the final value of ξ_{eqTOT} is slightly higher. In both cases the whole damping ratio is more than twice the typical value of the fixed base assuption.

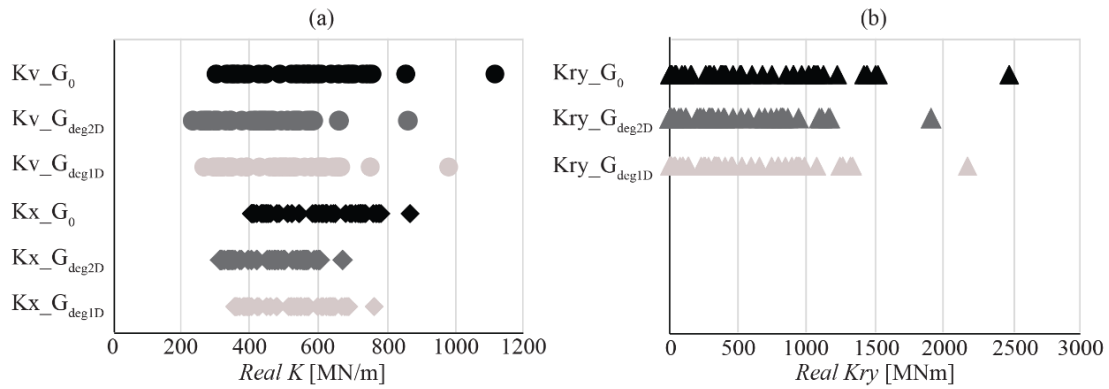

Figure 8. Range of variability of the real part of the foundation impedance, calibrated according to the initial soil stiffness (G_0) and the stiffness mobilized below the foundation according to the 1D (G_{deg1D}) and 2D (G_{deg2D}) site response analyses.

Table 2. Damping and equivalent damping of replacement oscillator, and final value used in the NLDA.

	D [%]				ξ_{eq} [%]				ξ_{eqTOT} [%]
	24th August		26th October		24th August		26th October		
	X	Y	X	Y	X	Y	X	Y	
1D	2.013	2.071	2.098	2.459	7.24	5.50	7.32	5.56	6.40
2D	3.597		3.029		8.59	6.72	8.10	6.27	7.42

5 COMPARISON AMONG THE SIMULATED AND OBSERVED DAMAGE

Since the aggregate is located at the edge of the valley, for a more accurate assessment of the damage, the acceleration time histories of the free field signals calculated along the X-axis in the vertical V3 through the 2D site response analyses, were applied together with the signals calculated through the 1D analyses in the Y-axis. The analyses were repeated also in the case in which, in both directions, the components of the input motion derived from 1D condition along V2 have been applied. Signals were thus applied to the FB model under free-field motions (named FB C case) and to the CB model under free-field motion (CB C case), to investigate the effects of the SFS interaction. In addition, the response of the FB model was also analysed under the bedrock motion, as a reference case, named FB A in the following, to evaluate only the effects of site amplifications. In all cases, the input motions relevant to the event occurred on the 24th August 2016 and 26th October 2016 were applied in cascade to simulate the cumulative damage.

Figure 9 compares the survey of the damage suffered by the main façade of the building with the outcomes of the NLDA at the end of the 26th October mainshock. This is the most vulnerable wall, due to the large openings at ground floor, while side perpendicular walls (being without openings and benefitting from the axial load transmitted by the diaphragms) are expected to be damaged lowly than the façade. As far the actual damage concerns, in Figure 9, the main pattern of cracks surveyed is reported together with a colour that indicated their severity (if lower than DL2, between DL2 and DL3 of higher). The damage level has been attributed on basis of the interpretation of available photos. Since it was not possible to enter the buildings, the damage has been assigned only from outside.

The comparison among the observed and simulated damage highlights that the FB A model considerably underestimates the damage, as many structural elements remain in the elastic range. That firstly confirms the role of amplification site effects. Conversely, the analysis performed on the FB model, under the 1D free-field signal, overestimates the damage producing the attainment of DL5 on piers at the ground floor. The CB C model without valley effect appears less damaged than the FB C model in the same hypothesis, but in any case, more damaged than the actual building.

When the free-field signals obtained from the 2D analyses are instead considered, the simulated damage is more close to the real one observed on the building both in the FB C and CB C model. As expected, both the valley effect and the SFS interaction have played a beneficial role in the seismic response of the aggregate.

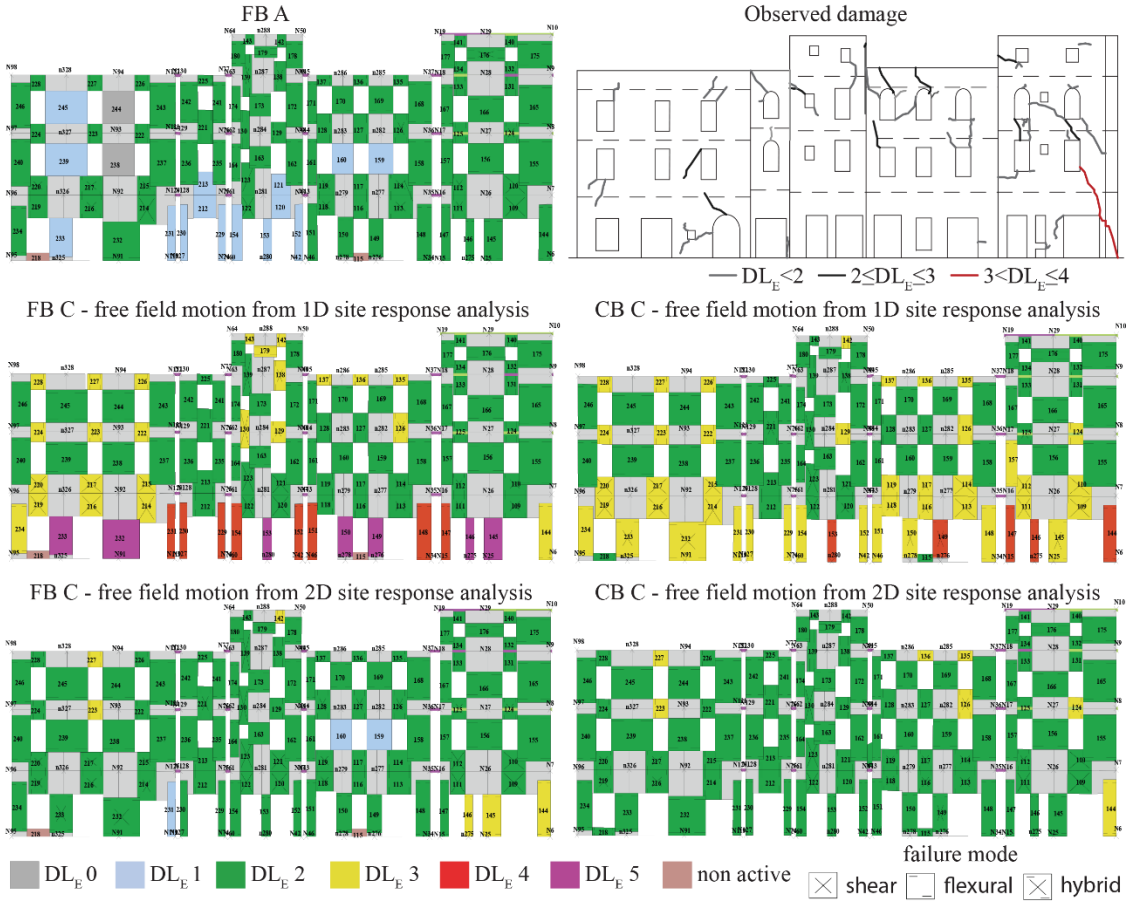

Figure 9. Comparison between observed and simulated damage on FB and CB model after the second mainshock.

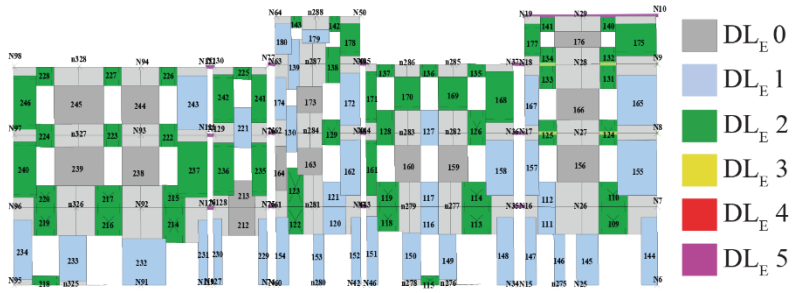

Figure 10. Simulated damage of CB model with valley effect before the peak of 24th August.

In fact, when the valley effect is considered, most of the structural elements are in DL2, apart the external ones in the unit U1 that already reached at least DL3, consistently with the observations. Despite that, in the real case there is a greater damage to the upper floors. This does not seem to be captured by the numerical model being everything in DL2. From Figure 6, DL2 of the numerical model corresponds to the attainment to the maximum shear strength of the panel, but the same DL may correspond to piers that just have been yielded or close to the attainment of DL3. In order to better investigate this aspect and discriminate to what condition the green colour actually corresponds to, Figure 10 shows the damage of the CB C model with the valley effect before the peak of 24th August. It is observed, consistently with the real damage, that the damage starts mostly on the upper floors and then spreads during the event on the lower floors.

6 CONCLUSION

The paper investigates the seismic response of URM building in aggregate. That architectural

type is quite relevant being the one most recurring in small historical centres, in Italy but more in general in Europe. Moreover, the effects of site amplification and SFS interaction are analysed with reference to the emblematic study case of Visso municipality, hit by the Central Italy 2016/2017 event. The historical centre of Visso is particularly interesting since it is founded on an alluvial valley and the topographic and morphological shape of the valley make relevant also the 2D effect. The comparison between the numerically simulated and real damage showed that:

- in case of soft soils, the role of amplification phenomena needs to be accounted for;
- in this case, to neglect the 2D effect leads to excessively conservative results;
- for the investigated URM buildings in aggregate, the effects of SFS interaction leads to a beneficial contribute.

7 REFERENCES

Alleanza, G.A., Chiaradonna, A., d'Onofrio, A., Silvestri, F. 2019. Parametric study on 2D effect on the seismic response of alluvial valleys. *Proc. of the 7th ICEGE, 17-20 June 2019*. Rome, Italy.

Alleanza, G.A. 2022. Two-Dimensional Amplification of Seismic Motion in Alluvial Valleys. Ph.D. dissertation. University of Napoli "Federico II", Napoli, Italy.

Angiolilli, M., Lagomarsino, S., Cattari, S., Degli Abbati, S. 2021. Seismic fragility assessment of existing masonry buildings in aggregate. *Engineering Structures* 247:113-218.

Brando, G., Pagliaroli, A., Cocco, G., Di Buccio, F. 2020. Site effects and damage scenarios: The case study of two historic centers following the 2016 Central Italy earthquake. *Engineering Geology* 272:105674.

Brunelli, A., de Silva, F., Piro, A., Sica, S., Parisi, F., Silvestri, F., Cattari, S. 2021. Numerical simulation of the seismic response and soil-structure interaction for a monitored masonry school building damaged by the 2016 Central Italy earthquake. *Bull Earthq Eng*. 19(2):1181-1211.

Brunelli, A., de Silva, F, Cattari, S. 2022. Site effects and soil-foundation-structure interaction: derivation of fragility curves and comparison with Codes-conforming approaches for a masonry school. *Soil Dyn. Earthq. Eng.* 154(4):107125.

Calderini, C., Cattari, S., Lagomarsino, S. 2009. In-plane strength of unreinforced masonry piers, *Earthquake Eng Struct Dyn* 38(2):243-67.

Caprili, S., Mangini, F., Salvatore, W., Scarpelli, G., Squeglia, N. 2015. The influence of soil–foundation–structure interaction on the overall behaviour and diseases of a medieval building in Pisa. *STREMAH 2015, 14th STREMAH, July 13-15 2015*, La Coruna, Spain.

Cattari, S. & Lagomarsino, S. 2013. *Masonry Structures* in Developments in the field of displacement based seismic assessment. Edited by Sullivan, T.J. & Calvi, G.M., IUSS Press, Pavia, Italy, pp.151-200 and EUCENTRE, pp. 524, ISBN; 978-88-6198-090-7.

Cattari, S., Camilletti, D., D'Altri, A.M., Lagomarsino, S. 2021. On the use of continuum Finite Element and Equivalent Frame models for the seismic assessment of masonry walls. *J. Build. Eng*. 43:102519.

Ciancimino, A., Lanzo, G., Alleanza, G. A., Amoroso, S., Bardotti, R., et al. 2020. Dynamic characterization of fine-grained soils in Central Italy by laboratory testing. *Bull. of Earthq. Eng*. 18:5503–5531.

D'Altri, A.M., Sarhosis, V., Milani, G., Rots, J., Cattari, S., Lagomarsino, S., Sacco, E., Tralli, A., Castellazzi, G., de Miranda, S. 2020. Modeling strategies for the computational analysis of unreinforced masonry structures: review and classification. *Arch. Comput. Methods Eng*. 27:1153-1185.

Gazetas, G. 1983. Analysis of machine foundation vibrations: state of the art. *Soil Dyn Earthq Eng*. 2:1-41.

Gazetas, G. 1991. Formulas and charts for impedances of surface and embedded foundations. *J Geotech Eng*, 117(9):1363-1381.

Hudson, M., Idriss, I.M., Beikae, M. 2003. *QUAD4M: a computer program to evaluate the seismic response of soil structures using finie element procedures and incorporating a compliant base, rev. 2003*. Center for Geotechnical Modelling Dept. of Civil and Environmental Engineering University of California, Devis.

Imai, T. & Yoshimura, Y. 1970. Elastic wave velocity and soil properties in soft soil. Tsuchito-Kiso 18 (1):17-22 (in Japanese).

Kottke, A. & Rathje, E.M.R. 2008. *Technical manual for Strata. Report No. 2008/10*. Pacific Earth-quake Engineering Research Center, University of California, Berkeley.

Kuhlemeyer, R.L. & Lysmer, J. 1973. Finite element method accuracy for wave propagation problems. *Soil Mechanics and Foundations*, 99(5):421–427.

Liao, T., Massoudi, N., Mchood, M., Stokoe, K.H., Jung, M. J., Menq, F.Y. 2013. Normalized Shear Modulus of Compacted Gravel. *Proc. 18th Int. Conf. on Soil Mech Geotech Eng. Challenges and Innovations in Geotechnics*, 1535–1538.

Lagomarsino, S., Penna, A., Galasco, A., Cattari, S. 2013. TREMURI program: An equivalent frame model for the nonlinear seismic analysis of masonry buildings. *Eng Struct*.56:1787-1799.

Lee, S.H.H. 1992. Analysis of the multicollinearity of regression equations of shear wave velocities. *Soils and Foundations* 32(1):205-214.

Maravas, A., Mylonakis, G., Karabalis, D.L. 2014. Simplified discrete systems for dynamic analysis of structures on footings and piles. *Soil Dyn Earthq Eng*, 61-62:29-39.

MIT. 2019. *Istruzioni per l'applicazione dell'aggiornamento delle Norme tecniche per le costruzioni* di cui al Decreto Ministeriale 17/01/2018, Ministry of Infrastructures and Transportations, Rome, Italy. (in Italian).

MZS3. 2018. *Report of the 3rd level Seismic Microzonation of Visso village*. Approved by the Working Group, May 29, 2018. https://www.comune.visso.mc.it/avvisi-cms/microzona-zione-sismica-iii-livello/.

NTC. 2018. *Norme Tecniche per le Costruzioni*. DM 17/01/2018, Italian Ministry of Infrastructure and Transportation, G.U. n. 42, 20 February 2018, Rome, Italy. (in Italian).

Ohta, Y. & Goto, N. 1978. Empirical shear wave velocity equations in terms of characteristic soil indexes. *Earthq. Eng. Struct. Dyn*. 6:167-187.

Ottonelli, D., Manzini, C.F., Marano, C., Cordasco, E.A., Cattari, S. 2021. A comparative study on a complex URM building: part I - sensitivity of the seismic response to different modelling options in the equivalent frame models. *Bull. Earthq. Eng.* https://doi.org/10.1007/s10518-021-01128-7.

Pagliaroli A., Pergalani F., Ciancimino A, Chiaradonna A., Compagnoni M., et al. 2020. Site response analyses for complex geological and morphological conditions: relevant case-histories from 3rd level seismic microzonation in Central Italy. *Bull. of Earthq. Eng.* 18:5741–5777.

Papadimitriou, A.G. 2019. An engineering perspective on topography and valley effects on seismic ground motion', *Proc. of the 7th ICEGE, 17-20 June 2019*. Rome, Italy.

Rezaie, A., Godio, M., Beyer, K. 2020. Experimental investigation of strength, stiffness and drift capacity of rubble stone masonry walls. *Construction and Building Materials* 251:118972.

Richart, F.E., Hall, J.R., Wood, R.D. 1970. *Vibrations of Soils and Foundations*. Prentice-Hall.

Sextos, A., De Risi, R., Pagliaroli, A., Pagliaroli, S., Foti, S., et al. 2018. Local site effects and incremental damage of buildings during the 2016 Central Italy Earthquake sequence. *Earthq Spectra*. 34(4):1639-1669.

Sorrentino, L., Cattari, S., da Porto, F., Magenes, G., Penna, A. 2019. Seismic behaviour of ordinary masonry buildings during the 2016 central Italy earthquakes. *Bull Earthq Eng.* 17(10):5583-5607.

Turnšek, V. & Sheppard, P. 1980. The shear and flexural resistance of masonry walls. *In Proc. Int. research conf earthq eng*. 30 *June – 3 July 1980*, Skopje, Macedonia.

Vanin, F., Zaganelli, D., Penna, A., Beyer, K. 2017. Estimates for the stiffness, strength and drift capacity of stone masonry walls based on 123 quasi-static cyclic tests reported in the literature. *Bull. Earth. Eng*, 15(12):5435-5479.